

**MINERALOGY OF MOUNT SHARP, GALE CRATER, USING ALONG TRACK OVERSAMPLED CRISM OBSERVATIONS TO SUPPORT PATH PLANNING FOR THE CURIOSITY ROVER.** V. K. Fox<sup>1</sup>, R. E. Arvidson<sup>1</sup>, and A. A. Fraeman<sup>2</sup> <sup>1</sup>Affiliation ([foxv@levee.wustl.edu](mailto:foxv@levee.wustl.edu)) Washington University in St Louis, Missouri, USA, <sup>2</sup>Jet Propulsion Laboratory, California Institute of Technology

**Introduction:** As the Curiosity Rover continues to explore the strata exposed on the slopes of Mt Sharp, strategic planning is crucial to ensure the efficient use of time and resources to achieve scientific goals. To this end, we have used MRO CRISM [1] full resolution targeted mode (FRT) and along-track oversampled (ATO) hyperspectral images regularized to 12 m/pixel to identify and map hematite, smectite, and hydrated sulfate deposits and their relative abundances for use in route planning. These maps are input to the strategic route planning and science teams to identify routes that are both possible from mobility perspectives and reach scientifically important outcrops.

**Data Processing:** CRISM products are processed to remove scene-specific atmospheric conditions, local topography, and detector behavior to produce high fidelity spatial projections and the best estimates of surface spectral reflectance (0.4 to 2.65  $\mu\text{m}$ ) in the presence of instrument noise.

*Atmospheric Modeling using DISORT.* Atmospheric and surface scattering processes are decoupled using DISORT. Gas absorptions, dominated by  $\text{CO}_2$ , are first removed using the standard volcano scan procedure. Dust and ice aerosol abundances are estimated from either off-nadir CRISM observations, measurements made by the Curiosity rover near the time of the CRISM observation, or estimated from climatological records. Aerosol scattering and absorption effects are then modeled with DISORT using the Hapke bidirectional surface reflectance function to retrieve single scattering albedo (SSA) values embedded in instrument-dependent noise. Local topography is modeled using MOLA gridded data.

*Log Maximum Likelihood Processing.* We apply an iterative maximum log-likelihood (MLM) algorithm to the SSA hyperspectral image cubes to retrieve the best estimate of true SSA values in the presence of Poisson noise and to project the ATO image cubes to 12 m/pixel, taking advantage of the along-track overlap of the 18 m wide pixels [2,3]. FRTs were regularized to the standard 18 m/pixel projections. The instrument's spatial and spectral transfer functions (modeled as Gaussian functions) are used to deblur the observed data, and the best estimate of the surface is updated iteratively to minimize the residuals between the measured and modeled data sets. Extrema values in the spectral domain, caused by noisy detector elements, are first removed using a median filter to ensure Poisson distributed noise.

Weighting penalties, adjusted as a function of wavelength and detector behavior, guarantee convergence. The increase in spatial fidelity for the MLM-processed ATOs is evident for scene ATO00021BC1 relative to the normal projection methods that do not invert the spatial transfer functions (Fig. 1)

*Mineral Mapping:* Standard CRISM parameter maps [4] were generated for each of the 13 scenes (7 FRTs and 6 ATOs) covering existing and planned Curiosity traverses (Fig. 2) to identify and map hematite, smectites, and hydrated sulfates (Fig. 3). These maps indicate the band depth of absorptions at wavelengths that are diagnostic of the specific mineral of interest. A deeper absorption can indicate a better surface exposure (i.e. the area is free from soil and dust cover), a change in mineral grain size, or a greater concentration of the mineral. Hematite (BD860), smectites (D2300) and hydrated sulfate (SIndex) maps were combined and overlain onto a co-registered HiRISE-based mosaic. These maps were produced by mosaicking the results of all relevant CRISM observations, after first setting minimum-value thresholds based on the aerosol opacities and detector temperatures for each scene. Maps were mosaicked in order of highest spatial resolution and lowest noise.

**Areas of Interest:** We focus on regions to be traversed by Curiosity, using a notional route that will be adjusted in planning and will become a broad corridor whose dimensions will be defined in part based on mineral maps presented in this abstract (Figs. 3-5).

*Hematite-capped Ridge:* The six CRISM observations that cover the hematite-rich ridge [5] show high hematite abundances on the southern-most edge of the east-west trending ridge. A north-jutting spur has the best surface exposure of hematite, and is within driving distance from Curiosity's likely traverse corridor.

*Smectite Trough:* The valley to the south of the hematite ridge shows the largest areal extent of smectite signatures, with high concentrations close to the nominal traverse and therefore likely well within any corridor.

*Fan Feature:* An enigmatic "fan" (alluvial fan, pediment?) extends from Mount Sharp and exhibits broad absorptions suggestive of ferrous silicates.

*Hydrated Sulfate Outcrops:* Above the smectite trough are layered hydrated sulfate-bearing strata. The sulfate signatures are wide-spread, indicating numerous locations where in-situ measurements can be made by Curiosity.



Figure 1 Use of scene ATO00021BC1 to illustrate the utility of the MLM approach for spatial regularization to 12 m/pixel. A. Projection of the data run through the MLM procedures without removing the spatial transfer functions and B. With inversion to remove the spatial transfer functions. L data are shown with RGB as 2.53, 1.50, and 1.06  $\mu\text{m}$ . Location of the scene is shown with green outline in Fig. 2B.

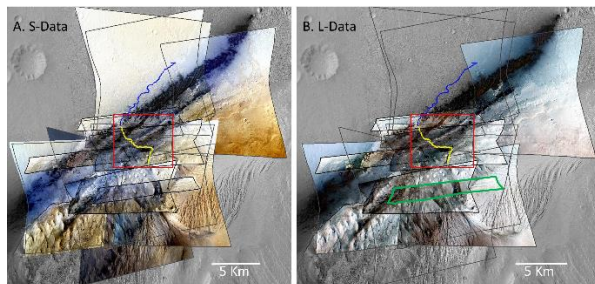


Figure 2: A) S-detector (0.39-1.05  $\mu\text{m}$ ) CRISM observations used in this study. There are 6 Along-Track Oversampled (ATO) observations, regularized to 12 m/pixel, and 7 Full-Resolution Targeted (FRT) observations, regularized to 18 m/pixel. B) All of the ATOs and 4 of the FRTs have corresponding L-data (1.03 – 2.65  $\mu\text{m}$ , this study). The blue line is the actual traverse route of the MSL Curiosity Rover through sol 1478, and the yellow line is the nominal extended mission route, which will be replaced with a broad corridor. Red boxes show area presented in Fig. 3.

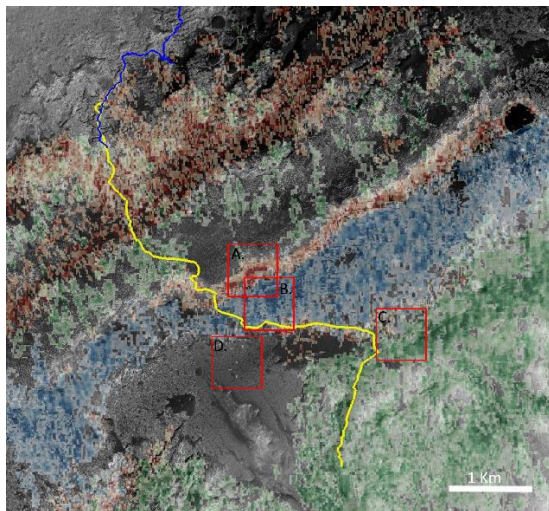


Figure 3: Composite maps showing the relative abundances of hematite (red), smectite (blue), and hydrated sulfate (green) in the region where Curiosity is expecting to traverse. Darker colors indicate a deeper absorptions and likely higher exposed concentrations. Red boxes indicate the areas shown in Figure 4.

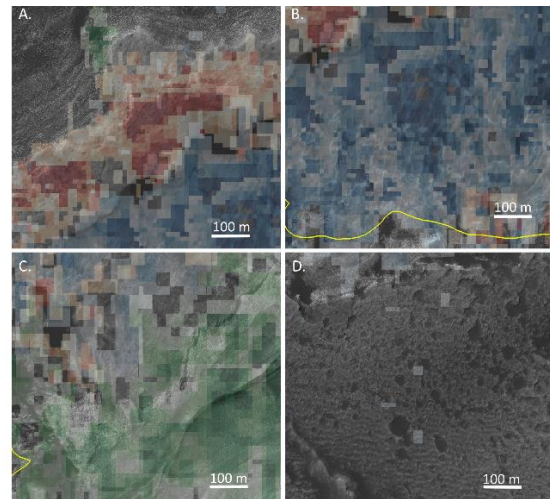


Figure 4: Regions that are candidates for exploration by Curiosity, showing mineral parameter maps. A. the hematite-capped ridge, B. the smectite valley, C. hydrated sulfate strata, and D. the “fan”. Locations for which spectra were retrieved are shown, with the data presented in Fig. 5.

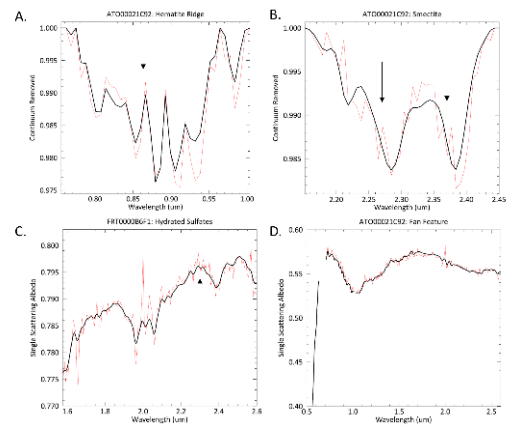


Figure 5: Means of 25 SSA spectra from the areas shown in Fig. 4, illustrating the absorptions mapped for hematite, smectites, and hydrated sulfates. Red lines represent data before extrema and MLM processing and black lines show final results from processing. Arrows indicate key wavelengths used for mineral identification. A) Hematite is detected by the presence an absorption at 0.86 $\mu\text{m}$ . The presence of basaltic sand can shift the absorption to slightly longer wavelengths. B) Smectite minerals are identified using metal-OH combination absorptions between 2.1 and 2.5  $\mu\text{m}$ . The band centers at 2.28 and 2.39 suggest iron-bearing smectites. C) Hydrated sulfates are parameterized by measuring the convexity at 2.29  $\mu\text{m}$ , to assess the presence of a pair of absorptions around 2.1 and 2.4 $\mu\text{m}$ . D) The “fan” feature is characterized only by broad absorptions suggestive of ferrous silicates.

**References:**

[1] Murchie, S., et al. (2007). *JGR*, 112, E05S03. [2] Kreisch, C.D. et al. (2017) *Icarus*, 282 136-151. [3] He, L., et al. *LPSC*, 2017 [4] Viviano-Beck, C. E. et al. (2014) *JGR-Planets.*, 119, 1403-1431. [5] Fraeman, A. A., et al. (2013) *Geology*, 41 1103-1106. [6] Fraeman, A. A., et al. (2016) *JGR-Planets*, 121.